Catalysis Today 342 (2020) 161–166

Contents lists available at ScienceDirect

Catalysis Today

journal homepage: www.elsevier.com/locate/cattod

Effect of proximity and support material on deactivation of bifunctional catalysts for the conversion of synthesis gas to olefins and aromatics

J.L. Weber[a], N.A. Krans[a], J.P. Hofmann[b], E.J.M. Hensen[b], J. Zecevic[a], P.E. de Jongh[a], K.P. de Jong[a,*]

[a] Inorganic Chemistry and Catalysis, Debye Institute for Nanomaterials Science, Utrecht University, Universiteitsweg 99, Utrecht, the Netherlands
[b] Laboratory of Inorganic Materials Chemistry, Department of Chemical Engineering and Chemistry, Eindhoven University of Technology, P.O. Box 513, 5600 MB Eindhoven, the Netherlands

ARTICLE INFO

Keywords:
Catalyst stability
Bifunctional catalyst
Fischer-Tropsch to olefins
Proximity
Synthesis gas to aromatics

ABSTRACT

Synthesis gas conversion to short olefins and aromatics using bifunctional catalysts has gained much attention in recent years. Here, we study the interaction between the components of bifunctional catalysts to design a more stable catalyst system. Mixing α-alumina supported iron (-carbide) promoted with sodium and sulfur with an H-ZSM-5 zeolite to convert synthesis gas to aromatics and short olefins we observed selectivity loss of the iron (-carbide) catalyst as well as the acid function. This was displayed by increasing methane and decreasing aromatics selectivity when the two individual catalysts were mixed in close proximity. We introduced different approaches to understand this selectivity related deactivation. Larger spatial separation of the iron and zeolite allowed a more stable system with constant methane and aromatics selectivity. Alternatively, iron supported on carbon nano tubes mixed with the zeolite in close proximity did not display selectivity related deactivation. We conclude that the selectivity loss was caused by migration of sodium ions that were used next to sulfur as promoters on the iron catalyst over the α-alumina support to the zeolite, which was supported by XPS model experiments. This migration seems hindered on carbon supported iron catalysts.

1. Introduction

Synthesis gas (a mixture of carbon monoxide/carbon dioxide and hydrogen) can be derived from coal [1] and natural gas [2] as well as from biomass [3] and can be converted to valuable chemicals such as short olefins and aromatics. This has received significant interest in the past years in academia and industry [4,5]. Recent publications have shown that bifunctional catalyst systems consisting of a metal oxide catalyst and a zeolite enable direct conversion of synthesis gas towards chemicals such as short olefins [6,7] and aromatics [8]. The intermediates in this reaction are reported to be oxygenates like methanol and dimethyl ether [9,10] or ketene [11].

Alternatively, cobalt carbide catalysts with certain crystal facets exposed or promoted iron (-carbide) based Fischer-Tropsch to olefins (FTO) catalysts can be used to convert synthesis gas to short olefins [12–18]. These catalysts show a selective suppression of methane formation next to an increase in olefins to paraffin ratio in the products and allows to form olefins in the range of C_2-C_4 beyond the Anderson-Schulz-Flory (ASF) distribution. In the case of iron (-carbide) based FTO catalysts, the presence of both sodium and sulfur promoters on the iron (-carbide) particles is essential for the decrease in methane selectivity [19–21].

In order to further convert the olefins formed on the iron (-carbide) based catalyst to aromatics the iron catalyst can be combined with a solid acid such as H-ZSM-5 zeolites in a single reactor [22–26]. The group of Ding successfully combined iron catalysts with an H-ZSM-5 zeolite to convert synthesis gas to aromatics with high CO conversion (85%) and aromatics selectivity (70% in C_{5+}). This was achieved by either impregnation of the zeolite with iron precursor or powder mixing of bulk iron catalysts with H-ZSM-5 zeolites [23,26]. Additionally, the group of Dadyburjor studied the effect of addition of H-ZSM-5 zeolite to carbon supported iron catalysts in different catalyst bed designs and observed catalyst deactivation in mixed bed mode, which was assigned to metal migration [24,25].

Typically, deactivation of supported metal catalysts has been ascribed to particle growth, which decreases the number of active sites but does not change their nature [27–30]. However, in bifunctional catalysts other deactivation mechanisms might play a role. For instance, a short distance between the iron (-carbide) and the acid sites of a bifunctional catalyst system may facilitate migration of alkali metal ions

* Corresponding author.
E-mail address: K.P.deJong@uu.nl (K.P. de Jong).

https://doi.org/10.1016/j.cattod.2019.02.002
Received 31 August 2018; Received in revised form 8 January 2019; Accepted 3 February 2019
Available online 04 February 2019

from the iron (-carbide) catalyst towards the zeolite [31] due to high mobility of alkali metal ions [32,33]. This could not only lower the activity and selectivity of the FTO catalyst but also neutralize the acid sites of the zeolite with alkali metal ions leading to a decreased selectivity to aromatization of olefins [34].

Here, we want to gain fundamental understanding of the mechanism of selectivity loss, with the final aim to allow design of more stable bifunctional catalysts. Therefore, we combined a Fischer-Tropsch to olefins (FTO) catalyst based on iron promoted with sodium and sulfur with an H-ZSM-5 zeolite to convert synthesis gas to aromatics with short olefins as intermediates [35]. This work focuses on both the influence of proximity [6,8,36] of the two catalytic functions as well as of the nature of the support on the stability. We show how the migration of promoters from the iron catalyst to the zeolite is affected and the resulting increase in methane selectivity and decreased selectivity to aromatics.

2. Experimental

2.1. Catalyst preparation

The promoted iron catalyst was prepared via incipient wetness impregnation of α-alumina (BASF, Al4196E, 7 m^2/g surface area, 0.4 mL/g pore volume (determined by water wetting). Prior to impregnation, the alumina powder was dried in a two-neck flask equipped with a vacuum valve adapter and a septum under vacuum at 120 °C for 2 h. After the flask was allowed to cool to 25 °C in vacuum the valve was closed, and the impregnation solution was added with a syringe and needle through the septum while stirring. The impregnation solution was prepared by dissolving ammonium ferric citrate (6.002 g, brown, Acros), sodium citrate monobasic (380.0 mg, Sigma Aldrich) and sulfuric acid (180.4 mg. 10 wt.-% solution in demineralized water) in demineralized water (20 mL). Three impregnation steps were necessary to achieve an iron loading of ˜6 wt.-%. Between the impregnation steps the material was dried under vacuum for 2 h at 60 °C. After the third impregnation step the samples were dried at 60 °C for 16 h in static air followed by calcination at 250 °C in static air for 4 h. The calcined iron catalyst was pelletized, ground and sieved to a fraction of 425–630 µm or 75–150 µm.

For the CNT supported iron catalyst, iron nano-crystals (Fe-NC) were prepared via colloidal synthesis. 1,2-hexadecandiol (350.9 mg), oleyl amine (214.9 mg), oleic acid (433.1 mg) and 1-octene (10 mL) were mixed in a 3-neck flask, equipped with a reflux condenser, septum and vacuum adapter connected to a Schlenk-line. Vacuum was applied, and the mixture was heated to 120 °C for 30 min. A mixture of iron pentacarbonyl (20.85 mg) and 1-octadecene (1 mL) was prepared in a nitrogen glovebox. The 3-neck flask was flushed with nitrogen three times followed by injection of the iron pentacarbonyl solution at 90 °C. The mixture was heated to 290 °C and kept there for 1 h. Afterwards the mixture was allowed to cool to 25 °C, it was transferred to a vial, to further process in air and mixed with an equal volume of *iso*-propanol. The Fe-NC were placed in a centrifuge (2700 rpm, 15 min) and the supernatant was decanted. 5 drops of toluene were added and the mixture was sonicated for 30 s, followed by a treatment in the centrifuge (2700 rpm, 15 min). The toluene-washing procedure was repeated. The as-synthesized Fe-NC were suspended in 10 mL 1-octadecene.

To attach the Fe-NC to the support the support material (CNT, Bayer BayTubes, 800 mg, surface area 230 m^2/g, pore volume 1.6 mL/g) was added into a 100 mL three-neck flask, which was connected to a Schlenk line through a reflux condenser. The suspended Fe-NC were added to the support material by pipetting while simultaneously magnetically stirring at 400 rpm. The mixture was brought under vacuum for 30 min at 120 °C to evaporate the toluene, and subsequently purged with nitrogen. The temperature was increased to 200 °C within 10 min under nitrogen flow and maintained for 30 min Afterwards, the mixture was allowed to cool down to 25 °C and further processed in air. Finally, the iron Fe-NP supported on the carbon materials were washed five times with hexane and acetone (hexane/acetone = 1:3 v/v) and dried at 60 °C for 1 h under static air, at 120 °C for 3 h under static air, and at 80 °C for 3 h under vacuum.

The addition of promoters to the CNT-supported Fe-NC was achieved using incipient wetness impregnation of the unpromoted Fe-NC after attachment to the CNT. The unpromoted Fe-NC on CNT were placed in a two-neck flask equipped with a septum and a vacuum valve adapter and heated to 60 °C under vacuum for 1 h. Afterwards the flask was allowed to cool to 25 °C (under vacuum) and the valve was closed. Sodium sulfide nonahydrate (212.5 mg) was dissolved in demineralized water (5.7 mL) and 1 mL of this solution was diluted with a mixture of water and *iso*-propanol (1:1 v/v, 9 mL of mixture). 1.2 mL of the final solution was added per gram of catalyst. The impregnated catalyst was dried under vacuum at 25 °C for 16 h and pelletized, ground and sieved to a fraction of 425–630 µm.

The ZSM-5 zeolite was transformed from the ammonium form (NH_4-ZSM-5, Zeolyst, Si:Al = 15 at/at) to the proton form H-ZSM-5 by calcination at 550 °C for 4 h in static air (the temperature programmed desorption profile of ammonia can be found in the supporting information, Fig. S1). Afterwards, the powder was pelletized, ground and sieved to a fraction of 425–630 µm or 75–150 µm.

The iron catalyst and the zeolite were combined with different proximities. In the stacked bed configuration (denoted as AFe + Z) the zeolite was placed downstream of the iron catalyst with a thin layer of silicon carbide in between. Mixed bed experiments were performed by physically mixing the iron catalyst and the zeolite in the reactor using sieve fractions of 75–150 µm (denoted as AFe/Z-100) and 425–630 µm (denoted as AFe/Z-500), respectively. To prepare composite catalysts consisting of the iron catalyst supported on alumina (denoted as AFeZ) and CNT (denoted as CFeZ), respectively, and the zeolite, the powders of the iron catalysts and the calcined zeolite were mixed in a mortar for 5 min to achieve an appropriate distribution within the final grains. The iron catalyst supported on alumina was mixed with the zeolite in a ratio of Fe/Al_2O_3:zeolite = 3:5 m/m, whereas the CNT-based iron catalysts were mixed with a ratio of Fe/CNT:zeolite = 4:5 m/m to compensate for the lower iron loading of the iron catalysts supported on CNT. Subsequently, the mixed powders were pelletized, ground and sieved to a fraction of 425–630 µm.

2.2. Characterization

The elemental composition of the calcined alumina-supported iron catalysts and the dried CNT-supported iron catalysts was determined with ICP analysis (supporting information, Table S1). Transmission electron microscopy (TEM) images were acquired using a FEI Talos F200X transmission electron microscope in bright field mode operating at 200 kV (supporting information, Figs. S2–S4). To analyze the porosity and surface area of the support materials, nitrogen physisorption was measured at liquid nitrogen temperature using a Micromeritics TriStar 3000 surface area and porosity analyzer. Prior to physisorption measurements, the alumina support was dried in nitrogen flow for 16 h at 300 °C and CNT support at 150 °C, respectively (isotherms and physisorption data can be found in the supporting information, Fig. S5 and Table S2).

X-ray photoelectron spectroscopy (XPS) measurements were carried out on a K-Alpha XP spectrometer (Thermo Scientific) equipped with a monochromatic small-spot (400 µm) X-ray source operating at 72 W, a 180° double focusing hemispherical analyzer with a 128-channel delay line detector and an Al anode (E(Al K_α) = 1486.6 eV). The background pressure inside the analysis chamber was kept below $8{\cdot}10^{-8}$ mbar reaching maximum of $3{\cdot}10^{-7}$ mbar during the measurements due to the flow of low energy Ar^+ ions involved in the charge neutralization process. Samples were handled in ambient air and were fixed on the XPS sample holder by conducting carbon tape. High-resolution spectra

of core levels (Al 2p, C 1s, Fe 2p, Na 1s, O 1s, Si 2p) and wide-range survey spectra were recorded with a pass energy of 50 eV and 200 eV, respectively. Binding energy calibration of the spectra was done by setting the C 1s peak of sp^3 adventitious carbon to 284.8 eV.

2.3. Catalytic performance

To analyze the catalytic performance of the α-alumina supported iron catalyst without zeolite, 15 mg of the calcined and sieved iron catalyst was loaded into a stainless-steel reactor with 2.6 mm inner diameter after dilution with 100 mg of silicon carbide. The stacked bed configuration was achieved by first loading 25 mg of calcined and sieved H-ZSM-5 zeolite diluted with 100 mg of silicon carbide into the reactor followed by a layer of silicon carbide to avoid direct contact between the iron catalyst and the zeolite. Afterwards, 15 mg of calcined and sieved iron catalyst was diluted with 100 mg of silicon carbide and loaded upstream of the zeolite into the reactor.

Mixed bed configurations were prepared by mixing 15 mg calcined and sieved iron catalyst, 25 mg calcined and sieved H-ZSM-5 zeolite and 200 mg silicon carbide in a glass vial, followed by loading the mixture into the reactor.

For the composite experiments of the α-alumina supported iron catalyst and zeolite, 40 mg of the sieved composite mixture was diluted with 150 mg silicon carbide and loaded into the reactor, whereas 45 mg of the composite of CNT supported iron catalyst and zeolite was loaded after dilution with 150 mg of silicon carbide.

The catalysts were tested in a 16-channel high throughput fixed bed reactor setup (Avantium Flowrence) by *in-situ* reduction of the calcined catalysts in a flow of 30% hydrogen in helium (v/v) at 350 °C for 2 h at 1 bar and a gas hourly space velocity (GHSV) of 10,500 h^{-1} followed by carburization in synthesis gas (CO/H_2 = 1 v/v, 5 $\%_{vol}$ He as internal standard) at 290 °C for 1 h at 1 bar and GHSV of 14,400 h^{-1}. The reaction conditions were 400 °C in synthesis gas (CO/H_2 = 1 v/v, 5 $\%_{vol}$ He as internal standard), 1 bar and GHSV of 14,400 h^{-1}. The GHSV is calculated based on the gas flow and the volume of the supported iron catalyst only. The C_1-C_9 hydrocarbon products as well as the permanent gases were analyzed with an online gas chromatograph equipped with a flame ionization detector (FID) and thermal conductivity detector (TCD). The reported selectivities were based on carbon atoms ($\%_C$) within hydrocarbon formed and were calculated excluding CO_2. The selectivity to CO_2 was in the range of the thermodynamic equilibrium of ~47% for all experiments.

A heat treatment to simulate a spent catalyst without the formation of coke on the surface for XPS measurements was performed by heating the calcined catalysts to 350 °C with 5 °C/min and hold for 2 h in a nitrogen flow with a GHSV of 10,500 h^{-1}, followed by 290 °C (5 °C/min) for 1 h in nitrogen flow with GHSV = 14,400 h^{-1} and 400 °C (5 °C/min) for 15 h in nitrogen flow with GHSV = 14,400 h^{-1}.

3. Results and discussion

3.1. Effect of proximity on catalyst stability

The sodium and sulfur promoted iron catalyst supported on α-alumina with an iron loading of 5.75 wt.-% (Na/Fe = 0.097 at/at, S/Fe = 0.0091 at/at) and 6.2 nm iron oxide particles was combined with an H-ZSM-5 zeolite in different configurations to vary the proximity between the iron catalyst and the zeolite (Fig. 1A). The iron time yield (moles of carbon monoxide converted per gram of iron and second) as a function of time can be found in Fig. 1B. The iron catalyst without zeolite (AFe) showed an iron time yield of 1.8×10^{-5} mol CO $g_{Fe}^{-1}\,s^{-1}$ at the beginning of the reaction decreasing to 1.2×10^{-5} mol CO $g_{Fe}^{-1}\,s^{-1}$ after 40 h on stream. The experiment performed in the stacked bed configuration (AFe + Z) showed similar activity, whereas the mixed bed configuration with large grain size (AFe/Z-500) had slightly higher FTY of 2.2×10^{-5} mol CO $g_{Fe}^{-1}\,s^{-1}$ at the beginning of the reaction, decreasing to 1.7×10^{-5} mol CO $g_{Fe}^{-1}\,s^{-1}$ after 40 h. In the experiment of the mixed bed configuration and small grain size (AFe/Z-100) a higher activity of 3.4×10^{-5} mol CO $g_{Fe}^{-1}\,s^{-1}$ was observed in the early stage of the reaction increasing to 3.9×10^{-5} mol CO $g_{Fe}^{-1}\,s^{-1}$ after 40 h. The composite mixture (AFeZ) showed an even higher activity in the beginning of 3.8×10^{-5} mol CO $g_{Fe}^{-1}\,s^{-1}$, decreasing to 2.7×10^{-5} mol CO $g_{Fe}^{-1}\,s^{-1}$ after 40 h.

In this set of experiments, we observed the trend that the initial activity increased with increasing proximity between the iron catalyst and the zeolite. In our previous work we found that this is caused by enhanced carburization of the iron catalyst when the iron catalyst is mixed with the zeolite in close proximity and observed full formation of iron carbide after 15 h under similar conditions [35]. The iron catalyst with the zeolite in a mixed bed configuration with small grains showed an increase in activity over time, in contrast to the other experiments that showed a gradual decrease. Using small grains in this experiment might have led to partial clogging of the catalyst bed due to coke formation under these conditions and therefore a gradual build-up of pressure of after ~10 h on stream.

The experiments performed with low proximity (AFe + Z and AFe/

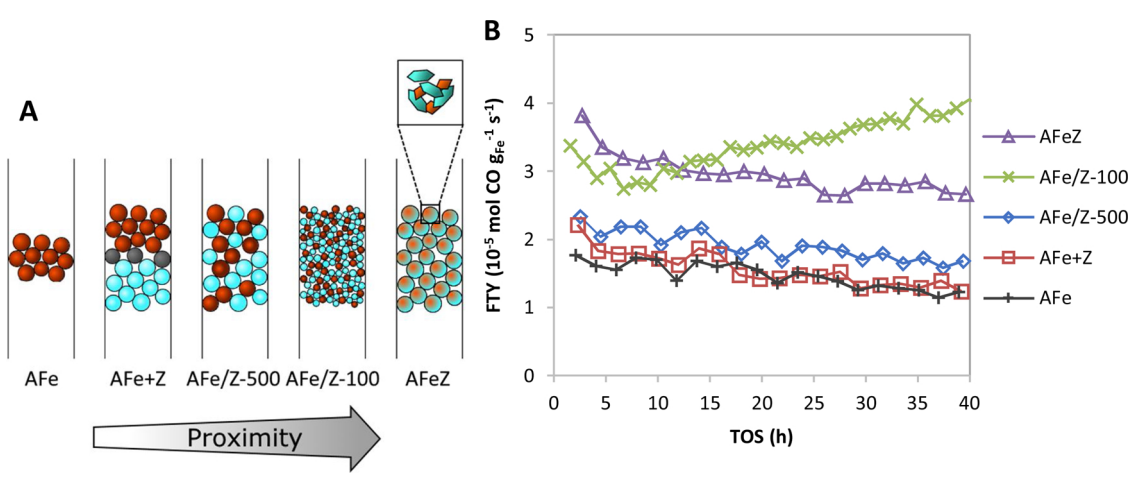

Fig. 1. A: Illustration of proximity between the iron catalyst and the zeolite. AFe: Iron catalyst without zeolite, AFe + Z: stacked bed with the zeolite downstream of the iron catalyst and a layer of silicon carbide between the two catalysts, AFe/Z-500 and AFe/Z-100: mixed bed configuration with the iron catalyst and the zeolite being mixed as a physical mixture with and average grain size of 500 µm and 100 µm, respectively and AFeZ: composite mixture of the iron catalyst and the zeolite. B: Iron time yield (FTY) of the iron catalyst as function of time on stream for samples with variable proximity between iron catalyst and zeolite. The higher the proximity between the iron catalyst and the zeolite, the higher the initial iron time yield. Reaction conditions: 400 °C, 1 bar, CO:H2 = 1 (v/v), GHSV: 14,400 h^{-1}.

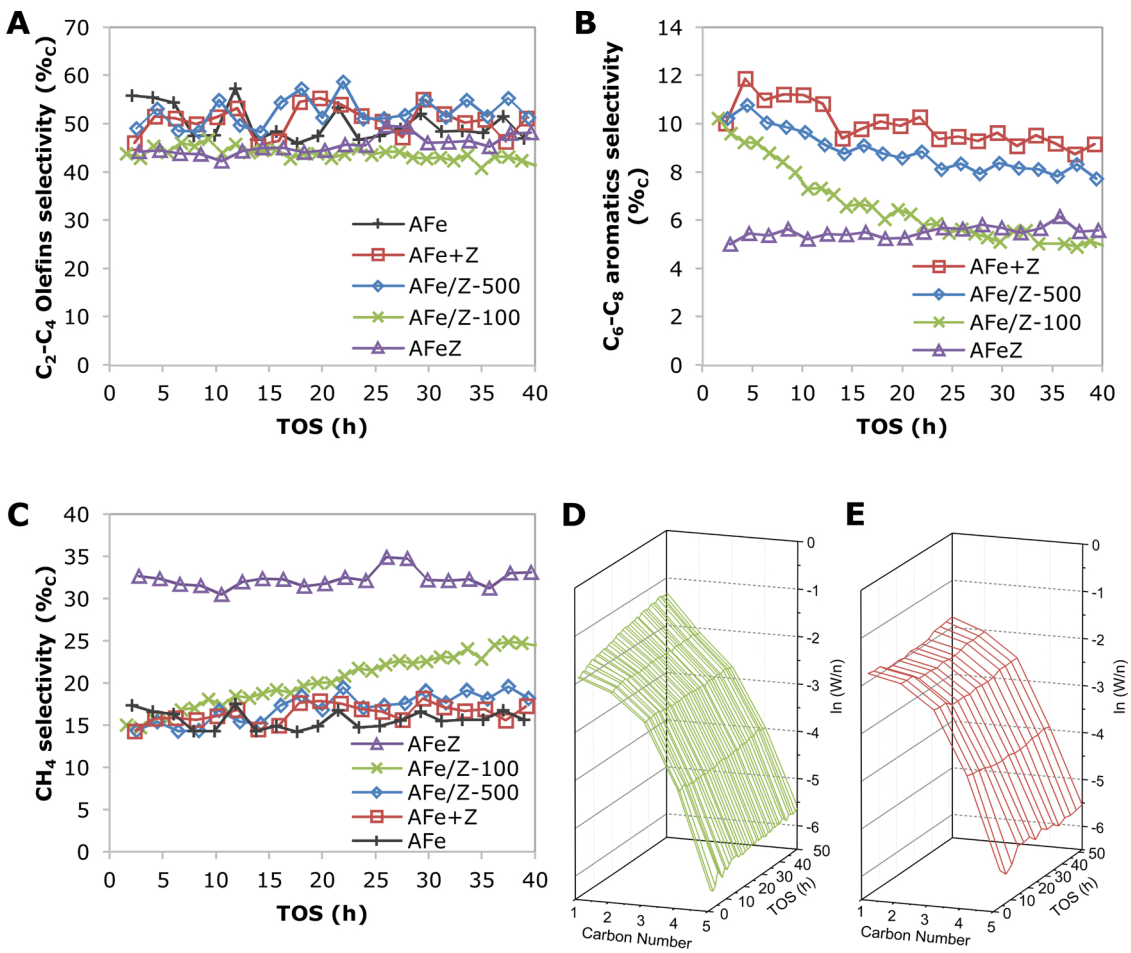

Fig. 2. A: Selectivity to C_2-C_4 olefins as function of time on stream (TOS) for the alumina supported iron catalyst mixed with the zeolite in different proximities. B: Selectivity to C_6-C_8 aromatics as function of time on stream for the alumina supported iron catalyst mixed with the zeolite in different proximities. C: Selectivity to methane as function of time on stream for the alumina supported iron catalyst mixed with the zeolite in different proximities. D: Anderson-Schulz-Flory distribution as function of time on stream for the iron catalyst mixed with the zeolite in a mixed bed configuration with small grain size (AFe/Z-100). E: Anderson-Schulz-Flory distribution as function of time on stream for the iron catalyst mixed with the zeolite in a stacked bed configuration (AFe + Z). Reaction conditions: 400 °C, 1 bar, $CO:H_2$ = 1 (v/v), GHSV: 14,400 h^{-1}. The selectivity to C_2-C_4 paraffins as a function of time can be found in Figure S6 in the supporting information.

Z-500) showed a selectivity to C_2-C_4 olefins of 49–59 $\%_C$, similar to the iron catalyst without zeolite (Fig. 2A). On the other hand, the experiments with higher proximity (AFeZ and AFe/Z-100) had lower C_2-C_4 olefin selectivity of 41–49 $\%_C$. The composite mixture of iron catalyst and zeolite showed a low selectivity to C_6-C_8 aromatics of only 5–6 $\%_C$ (Fig. 2B). The stacked bed and mixed bed experiments performed with lower proximity (AFe + Z and AFe/Z-500) displayed a decrease in selectivity to C_6-C_8 aromatics from 12 $\%_C$ to 9 $\%_C$ and 11 $\%_C$ to 8 $\%_C$ in the first 40 h of the experiment, respectively. The iron catalyst mixed with the zeolite in a mixed bed configuration and small grain size (AFe/Z-100) showed a strong decrease in C_6-C_8 aromatic selectivity from 10 $\%_C$ to 6 $\%_C$ in the first 18 h followed by further decrease to 5 $\%_C$ after 40 h on stream. The methane selectivity of the iron catalyst without zeolite (AFe), the stacked bed configuration (AFe + Z) and the mixed bed with large grain size (AFe/Z-500) was between 14 $\%_C$ and 19 $\%_C$ throughout the whole experiment (Fig. 2C). The composite mixture (AFeZ) had high methane selectivity of 31 $\%_C$ to 35 $\%_C$, whereas the methane selectivity of the mixed bed mixture of iron catalyst and zeolite with small grain size (AFe/Z-100) increased from 15 $\%_C$ to 25 $\%_C$ after 40 h.

In Fig. 2D and E the ASF-distribution for (aliphatic) C_1-C_5 hydrocarbons as a function of time on stream of the mixed bed experiment with small grain size (AFe/Z-100) and the stacked bed experiment (AFe + Z) can be seen, respectively. Here, the natural logarithm of the molar product fraction per carbon number was plotted versus the corresponding carbon number as a function of time on stream. The ideal ASF distribution would show a straight line. However, the presence of sodium and sulfur on an iron catalyst can break the ASF-distribution by selectively suppressing the methane formation as well as increase the olefin/paraffin ratio in the product distribution [19,37].

The mixed bed experiment with small grain size (AFe/Z-100) showed this suppression of methane formation in the beginning of the reaction. As the reaction progressed, the product distribution converged towards the ideal ASF-distribution. The experiment with the stacked bed configuration (AFe + Z) showed the altered product distribution with suppressed methane formation throughout the whole experiment.

These data show that the proximity between the iron catalyst and the zeolite has a limited influence on the selectivity of the bifunctional catalyst for olefins whereas the effects on aromatics and methane selectivities are significant. The ASF-distribution as function of time on stream for the mixed bed experiment with small grain size (Fig. 2D) suggests a gradual loss of the effect of sodium and sulfur promoters on the iron catalyst over time, whereas this loss of promoter effect was not observed for the spatially separated stacked bed experiment (Fig. 2E). This is in line with the selectivity of methane and C_2-C_4 olefins over time, where the stacked bed experiment showed stable selectivities in the range of the iron catalyst without zeolite for methane as well as for C_2-C_4 olefins and the mixed bed experiment with small grains displayed an increasing methane selectivity over time as well as a lower C_2-C_4 olefin selectivity. Furthermore, the decrease over time in selectivity to

C_6-C_8 aromatics for AFe/Z-100 indicates a gradual migration of sodium ions from the iron catalyst to the zeolite resulting in neutralization of acid sites in the zeolite. The composite mixture of the iron catalyst and the zeolite displayed a low selectivity to C_6-C_8 aromatics from the beginning of the reaction, which suggests fast migration of sodium ions from the iron catalyst to the zeolite due to the close proximity of the iron and the zeolite. This is also in agreement with the high methane selectivity for the composite mixture from the beginning of the reaction.

To provide spectroscopic evidence for the migration of sodium ions from the iron catalyst to the zeolite, we performed X-ray photoelectron spectroscopy (XPS) measurements on the calcined iron catalyst without zeolite and the mixed bed mixture of the iron catalyst and zeolite with small grains after heat treatment. The catalysts were treated using the same temperature profile as for the catalytic performance measurement (5 °C/min to 350 °C, 2 h; 5 °C/min to 290 °C, 1 h; 5 °C/min to 400 h, 15 h). However, we used an inert nitrogen flow to avoid carbon formation on the surface of the catalysts during catalysis, which would interfere with the XPS measurement due to screening of photoelectrons. A sodium ion exchanged ZSM-5 zeolite (denoted as Na-ZSM-5) was analyzed as a reference for sodium ions being located in the zeolite. The calcined iron catalyst initially showed a Na 1 s signal in XPS at 1071.4 eV, whereas the position of this peak did not change upon performing the heat treatment (Fig. 3). However, the mixed bed mixture of the iron catalyst and the zeolite after the heat treatment showed a shift of the Na 1 s signal to 1073.0 eV, which is in the range of the sodium ion exchanged zeolite (1072.8 eV). This shift towards higher binding energy of the signal for the Na 1 s electrons after the heat treatment supports our hypothesis of migration of sodium ions from the iron catalyst to the zeolite, resulting in loss of promotion effect on the iron catalyst as well as decreased acidity of the zeolite.

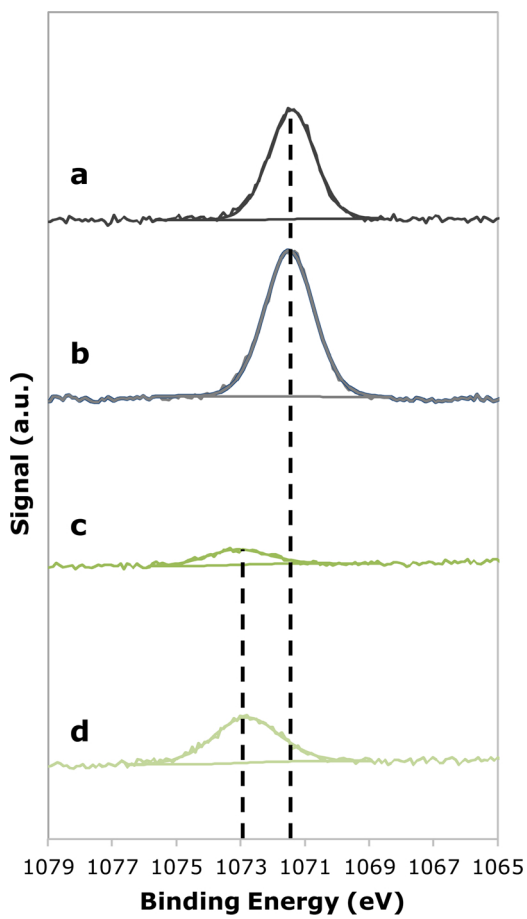

Fig. 3. X-ray photoelectron spectra of the Na 1 s core level region of (a) the α-alumina supported iron catalysts without zeolite, (b) the α-alumina supported iron catalysts without zeolite after heat treatment, (c) α-alumina supported iron catalysts and zeolite in mixed bed configurations with 75–150 µm grains size after heat treatment, and (d) sodium ion exchanged ZSM-5 zeolite.

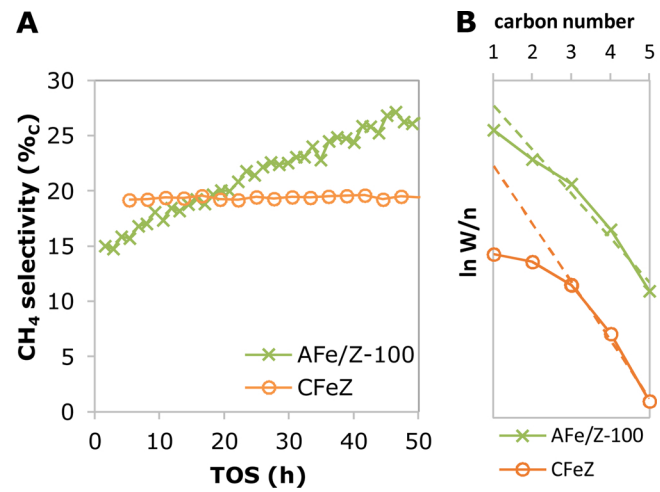

Fig. 4. A: Methane selectivity of the sodium and sulfur promoted iron catalyst supported on CNT in a composite mixture with the zeolite (CFeZ) and the α-alumina supported sodium and sulfur promoted iron catalyst in a mixed bed configuration with the zeolite and 75–150 µm grain size (AFe/Z-100) as a function of time on stream, B: Anderson-Schulz-Flory distribution for the sodium and sulfur promoted iron catalyst supported on CNT in a composite mixture with the zeolite (CFeZ) after 100 h on stream and the α-alumina supported sodium and sulfur promoted iron catalyst in a mixed bed configuration with the zeolite and 75–150 µm grain size (AFe/Z-100) after 50 h on stream. Reaction conditions: 400 °C, CO/H_2 = 1, GHSV = 7200 h^{-1}, 1 bar.

3.2. Effect of support material on catalyst stability

To study the effect of support material on the stability, an iron catalyst supported on carbon nano-tubes (CNT) was prepared by attaching colloidal iron nano-crystals (Fe-NC) onto CNT [38,39], followed by incipient wetness impregnation with a solution that contained sodium and sulfur promoters (resulting in 2.96 wt.-% Fe, Na/S = 0.073 at/at, S/Fe = 0.036 at/at, 8.4 nm iron oxide particles). The iron loading was limited to 3 wt-% to avoid fast deactivation due to sintering of Fe-NC [39]. This CNT supported iron catalyst was used to prepare a composite mixture with the H-ZSM-5 zeolite (denoted as CFeZ). This composite catalyst demonstrated a lower overall stability (supporting information, Fig. S7) but constant selectivity to methane of 19 $\%_C$ throughout the runtime of 50 h (Fig. 4A). In comparison, the alumina supported iron catalyst in a mixed bed configuration with the zeolite and small grain size showed that the methane selectivity increased from 15 $\%_C$ to 27 $\%_C$. The ASF distribution of these two experiments after 50 h on stream for the alumina supported iron catalyst in a mixed bed configuration with the zeolite and small grains and after 100 h on stream for the composite with the CNT-supported iron catalyst and zeolite can be seen in Fig. 4B, respectively. The CNT-supported iron catalyst as composite with the zeolite showed a strong deviation from the ASF distribution with lower methane selectivity, whereas for the alumina supported iron catalyst in a mixed bed with the zeolite this deviation was much less pronounced. This constant selectivity of the composite mixture of the CNT-supported iron catalyst and the zeolite indicates that the migration of sodium ions over the surface of the support towards the zeolite is hindered, despite the close proximity of iron and zeolite. We hypothesize that the migration of sodium ions over the CNT surface was hindered due to the limited capability of the CNT material for charge compensation of the sodium ions moving from the iron (-carbide) to the zeolite.

An increased methane selectivity due to the loss of promotion effect on the iron (-carbide) function as well as decreased selectivity to C_6-C_8 aromatics caused by neutralization of acid sites of the zeolite by sodium ions was observed when the iron catalyst was mixed with the zeolite in close proximity. The migration of sodium ions from the iron catalyst to the zeolite was confirmed using XPS. Mixing the iron catalyst and the zeolite in lower proximity prevented this loss of promotion effect and decrease in acidity of the zeolite, due to the spatial separation of the two catalysts. Furthermore, our hypothesis of sodium ion migration from the iron catalyst to the zeolite was supported by using carbon as support material for the iron catalyst, which is suggested to lack the capability of charge compensation for diffusing sodium ions.

4. Conclusions

We combined an α-alumina supported iron catalyst promoted with sodium and sulfur with an H-ZSM-5 zeolite to convert synthesis gas to olefins and aromatics in a single reactor. The presence of both sodium and sulfur on the iron catalyst led to a deviation from the Anderson-Schulz-Flory distribution with decreased methane selectivity. However, when the iron catalyst was mixed with the zeolite in close proximity, the deviation from the ASF-distribution vanished over time and the selectivity to methane increased, whereas the selectivity to aromatics decreased. We attributed this behavior to the migration of sodium ions from iron to zeolite, resulting in a loss of promotion effect of iron and neutralization of acid sites in the zeolite. The migration of sodium ions as a result of heat treatment was confirmed using XPS. Catalysis with lower proximity of iron and zeolite circumvented the migration of sodium ions. Furthermore, using carbon material as support for the iron catalyst supported our hypothesis of sodium ion migration. Possibly due to limited capability of charge compensation of moving sodium ions, their migration was hindered over the carbon support. These findings are important for future development of more stable bifunctional catalyst systems.

Declaration of interest

The authors declare no conflict of interest.

Acknowledgements

This work was supported by the Netherlands Center for Multiscale Catalytic Energy Conversion (MCEC), an NWO Gravitation program funded by the Ministry of Education, Culture and Science of the government of the Netherlands. KPdJ, JZ and NAK acknowledge the European Research Council, EU FP7 ERC Advanced Grant no. 338846. This project has received funding from the European Research Council (ERC) under the European Union's Horizon 2020 research and innovation programme ERC-2014-CoG 648991. Tiny Verhoeven and Longfei Wu (Eindhoven University of Technology) are thanked for their assistance in performing XPS measurements.

Appendix A. Supplementary data

Supplementary data associated with this article can be found, in the online version, at https://doi.org/10.1016/j.cattod.2019.02.002.

References

[1] J.J. Hernández, G. Aranda-Almansa, C. Serrano, Energy Fuels 24 (2010) 2479–2488.
[2] I. Dybkjaer, Fuel Process. Technol. 42 (1995) 85–107.
[3] J.J. Hernández, G. Aranda-Almansa, A. Bula, Fuel Process. Technol. 91 (2010) 681–692.
[4] M. Peters, B. Köhler, W. Kuckshinrichs, W. Leitner, P. Markewitz, T.E. Müller, ChemSusChem 4 (2011) 1216–1240.
[5] D.J. Roddy, Appl. Therm. Eng. 53 (2013) 299–304.
[6] F. Jiao, J. Li, X. Pan, J. Xiao, H. Li, H. Ma, M. Wei, Y. Pan, Z. Zhou, M. Li, S. Miao, J. Li, Y. Zhu, D. Xiao, T. He, J. Yang, F. Qi, Q. Fu, X. Bao, Science 351 (2016) 1065–1068.
[7] U. Olsbye, Angew. Chem. - Int. Ed. 55 (2016) 7294–7295.
[8] K. Cheng, W. Zhou, J. Kang, S. He, S. Shi, Q. Zhang, Y. Pan, W. Wen, Y. Wang, Chem. 3 (2017) 334–347.
[9] K. Cheng, B. Gu, X. Liu, J. Kang, Q. Zhang, Y. Wang, Angew. Chem. - Int. Ed. 55 (2016) 4725–4728.
[10] W. Zhou, J. Kang, K. Cheng, S. He, J. Shi, C. Zhou, Q. Zhang, J. Chen, L. Peng, M. Chen, Y. Wang, Angew. Chem. Int. Ed. (2018), https://doi.org/10.1002/anie.201807113.
[11] F. Jiao, X. Pan, K. Gong, Y. Chen, G. Li, X. Bao, Angew. Chem. Int. Ed. 57 (2018) 4692–4696.
[12] L. Zhong, F. Yu, Y. An, Y. Zhao, Y. Sun, Z. Li, T. Lin, Y. Lin, X. Qi, Y. Dai, L. Gu, J. Hu, S. Jin, Q. Shen, H. Wang, Nature 538 (2016) 84–87.
[13] F. Yu, T. Lin, X. Wang, S. Li, Y. Lu, H. Wang, L. Zhong, Y. Sun, Appl. Catal. A Gen. 563 (2018) 146–153.
[14] J. Xie, J. Yang, A.I. Dugulan, A. Holmen, D. Chen, K.P. de Jong, M.J. Louwerse, ACS Catal. 6 (2016) 3147–3157.
[15] H.M. Torres Galvis, K.P. de Jong, ACS Catal. 3 (2013) 2130–2149.
[16] M. Oschatz, T.W. van Deelen, J.L. Weber, W.S. Lamme, G. Wang, B. Goderis, O. Verkinderen, A.I. Dugulan, K.P. de Jong, Catal. Sci. Technol. 6 (2016) 8464–8473.
[17] H.M. Torres Galvis, J.H. Bitter, C.B. Khare, M. Ruitenbeek, A.I. Dugulan, K.P. de Jong, Science 335 (2012) 835–838.
[18] X. Wang, W. Chen, T. Lin, J. Li, F. Yu, Y. An, Y. Dai, H. Wang, L. Zhong, Y. Sun, Chin. J. Catal. 39 (2018) 1869–1880.
[19] H.M. Torres Galvis, A.C.J. Koeken, J.H. Bitter, T. Davidian, M. Ruitenbeek, A.I. Dugulan, K.P. de Jong, J. Catal. 303 (2013) 22–30.
[20] M. Oschatz, N. Krans, J. Xie, K.P. de Jong, J. Energy Chem. 25 (2016) 985–993.
[21] F. Jiang, M. Zhang, B. Liu, Y. Xu, X. Liu, Catal. Sci. Technol. 7 (2017) 1245–1265.
[22] B. Zhao, P. Zhai, P. Wang, J. Li, T. Li, M. Peng, M. Zhao, G. Hu, Y. Yang, Y.W. Li, Q. Zhang, W. Fan, D. Ma, Chem. 3 (2017) 323–333.
[23] Y. Xu, J. Liu, G. Ma, J. Wang, J. Lin, H. Wang, Fuel 228 (2018) 1–9.
[24] A.V. Karre, A. Kababji, E.L. Kugler, D.B. Dadyburjor, Catal. Today 198 (2012) 280–288.
[25] A.V. Karre, A. Kababji, E.L. Kugler, D.B. Dadyburjor, Catal. Today 214 (2013) 82–89.
[26] Y. Xu, J. Liu, G. Ma, J. Wang, Q. Wang, J. Lin, H. Wang, C. Zhang, M. Ding, Mol. Catal. 454 (2018) 104–113.
[27] C.H. Bartholomew, Appl. Catal. A Gen. 212 (2001) 17–60.
[28] C. Hernández Mejía, C. Vogt, B.M. Weckhuysen, K.P. de Jong, Catal. Today (2018), https://doi.org/10.1016/j.cattod.2018.11.036.
[29] G. Prieto, J. Zečević, H. Friedrich, K.P. de Jong, P.E. de Jongh, Nat. Mater. 12 (2013) 34–39.
[30] C.E. Pompe, M. Slagter, P.E. de Jongh, K.P. de Jong, J. Catal. 365 (2018) 1–9.
[31] F.G. Botes, W. Böhringer, Appl. Catal. A Gen. 267 (2004) 217–225.
[32] J.B. Goodenough, H.-P. Hong, J.A. Kafalas, Mat. Res. Bull. 11 (1976) 203–220.
[33] B.L. Ellis, W.R.M. Makahnouk, W.N. Rowan-Weetaluktuk, D.H. Ryan, L.F. Nazar, Chem. Mater. 22 (2010) 1059–1070.
[34] X.Y. Gwagwa, E. van Steen, Chem. Eng. Technol. 32 (2009) 826–829.
[35] J.L. Weber, I. Dugulan, P.E. de Jongh, K.P. de Jong, ChemCatChem 10 (2018) 1107–1112.
[36] J. Zecevic, G. Vanbutsele, K.P. de Jong, J.A. Martens, Nature 528 (2015) 245–254.
[37] H.M. Torres Galvis, A.C.J. Koeken, J.H. Bitter, T. Davidian, M. Ruitenbeek, A.I. Dugulan, K.P. de Jong, Catal. Today 215 (2013) 95–102.
[38] N.A. Krans, E.C. van der Feltz, J. Xie, A.I. Dugulan, J. Zečević, K.P. de Jong, ChemCatChem 10 (2018) 3388–3391.
[39] M. Casavola, J. Hermannsdörfer, N. De Jonge, A.I. Dugulan, K.P. De Jong, Adv. Funct. Mater. 25 (2015) 5309–5319.